Timing and Spacing Control in Microchannel Flow by Applying Periodic Force over Space and Time

AUTHOR(S):

Tatsumi, Kazuya; Noma, Atsushi; Honma, Renato; Kuriyama, Reiko; Nakabe, Kazuyoshi

CITATION:

Tatsumi, Kazuya ...[et al]. Timing and Spacing Control in Microchannel Flow by Applying Periodic Force over Space and Time. Microfluidics and Nanofluidics 2021, 25(2): 15.

ISSUE DATE:

2021-02

URL:

http://hdl.handle.net/2433/269395

Particle Timing and Spacing Control in Microchannel Flow by Applying Periodic Force over Space and Time

Kazuya Tatsumi*, Atsushi Noma, Renato Honma,
Reiko Kuriyama and Kazuyoshi Nakabe

Department of Mechanical Engineering and Science, Kyoto University,
Kyotodaigakukatsura, Kyoto, Kyoto 615-8450, Japan.

Corresponding Author
**E-mail: tatsumi@me.kyoto-u.ac.jp*
ORCID: 0000-0001-9993-9234

Abstract

This study develops a technique to control the timing, spacing (interval), and velocity of particles in a microchannel flow by periodically exerting forces on the particles over space and time. The periodic force was produced by dielectrophoretic force using boxcar-shaped electrodes on the channel wall. We could define the timing, interval, and velocity of the particles by configuring the on–off cycles of the applied voltage. Controlling the particle spacing and timing when it crosses a position in the channel and the focusing effect in the cross-sectional position could improve the performance and throughput of microfluidics, particularly for sensing, active sorting, and encapsulation of particles and cells. The proposed technique was first evaluated by a one-dimensional analysis based on a perturbation theory. We conducted a numerical simulation to solve the dielectrophoretic force distribution and the equation of motion of the particles to understand the relationship between the force and the particle motion in the boxcar-electrode region. We measured the velocity and position of the micro-particles flowing over the boxcar-electrode region in the microchannel and demonstrated the performance and accuracy of the proposed technique for alignment and timing control. The probability density functions (PDFs) of the period between the particles, particle velocity, and timing, concentrated at the target value with minimal variation. Furthermore, the measurement of particles with diameters of 8, 10, and 12 μm resulted in the same PDFs, which showed the applicability to a reasonable variation of particle diameters.

Keywords Particle alignment, Timing control, Dielectrophoretic force, Periodic force, Microchannel flow

1. Introduction

Controlling the timing of the particles passing a certain position in the flow and interval (space) between the particles in the microchannel flow is an important technique in the fields of engineering, biology, and medicine. For example, in microfluidic devices, we need to control the position of the particles

and focus them at a certain position in the cross-section of the microchannel to make each particle flow through the specific area and perform the sensing, sorting, and encapsulation accurately. It is essential to control the interval (space) between the particles and the timing when they pass the specific region in the microchannel to increase the performance as multiple particles entering the region or deviation in the timing can lead to signal and manipulation errors (Sun et al. 2007; Edd et al. 2008; Baret et al.; 2009; Abate et al. 2009; Guo et al. 2010; Cheung et al. 2010; Chen et al. 2013; Lagus and Edd 2013; Schoeman et al. 2014; Shields et al. 2015; Yan et al. 2017, Zhang et al. 2020).

Many techniques have been developed to control the particle position and focus them in the channel cross-section using the fluid dynamic lift force (Di Carlo et al. 2007; Oakey et al. 2010; Xuan et al. 2010; Ahn et al. 2011; Kemna et al. 2012; Chung et al. 2013; Gao et al. 2017; Lu et al. 2017; Dietsche et al. 2019; Yuan et al. 2019; Garcia and Pennathur 2019), electrokinetic forces (Fiedler et al. 1998; Cui et al. 2001; Hughes 2002; Zhu et al. 2009; Tatsumi et al. 2016), acoustic force (Laurell et al. 2007; Wood et al. 2008, Yigit et al. 2020), magnetic force (Afshar 2011), and optical forces (Čižmár et al. 2006). We can also statically order (align) the particles with even spacing in the spanwise and streamwise directions by applying a force distribution with a local minimum generated by a periodic force pattern as a standing wave type force distribution. The force distribution can be generated by periodic patterns of electric (Cui et al. 2001) and optical forces (Zemánek 2003; Garcés-Chévez 2005; Čižmár 2006; Sun et al. 2007) to align the particles in the channel or wall near the region. An acoustic standing wave is another way to produce the periodic force distribution in the channel (Wood et al. 2008, Yigit et al. 2020).

It is more challenging to control the streamwise position of the particles flowing in the channel and aligning them as they flow. One technique to control the spacing between the particles in a microchannel flow is the so-called inertial microfluidic technique, which uses the fluid dynamic force and secondary flows. The particles focus in a specific position at which the lift force, centrifugal force, and particle-induced fluid dynamic force balance, and the stagnation point to which the particles are convected (Di Carlo 2007; Oakey et al. 2010; Ahn et al. 2011; Kemna et al. 2012; Chung et al. 2013; Gao 2017; Lu et al. 2017, Hu et al. 2020). Using viscoelastic fluid and power-law fluid, the flow produces additional force to align the particles in the flow (D'Avino et al. 2020; Giudice et al. 2018; Hu et al. 2019). Furthermore, several other phenomena are also found in nature that convect and concentrate particles, cells, species, and molecules with equal spacing. Typical examples are the periodic force distributions that move like a traveling wave (Feynman 1949; Borromeo and Marchesoni 1998; Constantin 2006; Lewis and Guy 2017; Chen et al. 2019; Zhang et al. 2019). Particles can be carried by the free fluid surface (Fedele et al. 2016), acoustic (Coakley et al. 1989), optical (Koss and Grier 2003; Lozano and Bechinger), electric (Morgan et al. 1997; Zhu et al. 2009), and magnetic waves (Tierno and Straube 2016) with spacing equal to the wavelength. The Brownian ratchet (thermal ratchet) can also be considered as an alignment technique for molecules and particles in a flow (Magnasco 1993; Rousselet et al. 1994; Faucheux et al. 1995; Jűlicher et

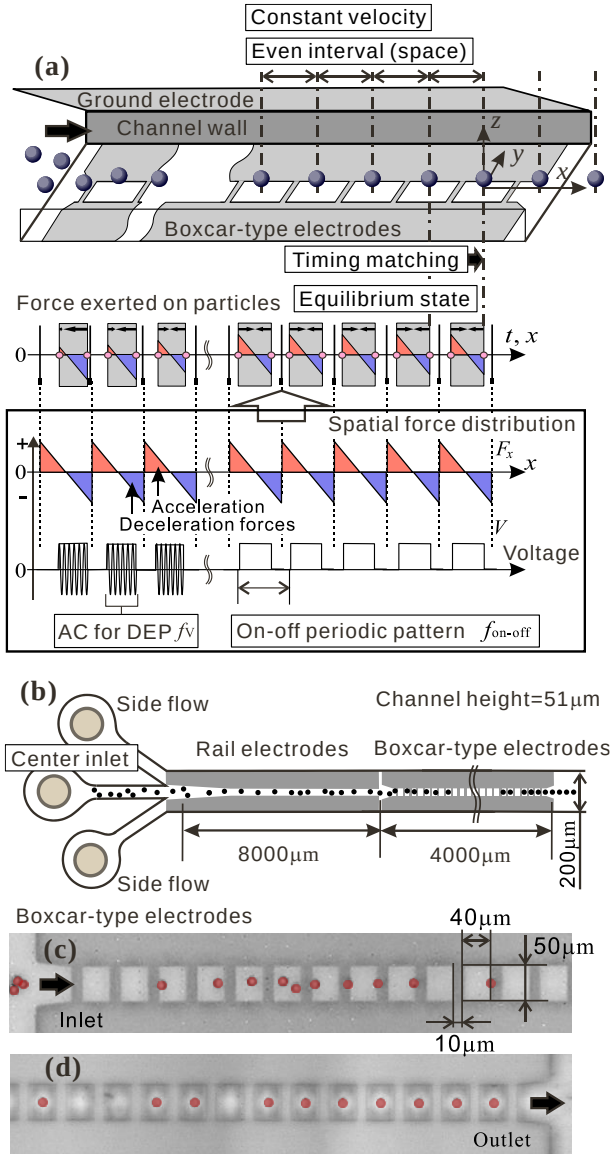

Fig. 1. (a) Schematic of the boxcar-type electrodes, microchannel, and the force exerted on the particles by the combination of the periodic force distribution in the streamwise direction and the on-off cycle of the applied voltage. (b) Overview of microchannel and electrode positions. (c) and (d) Snapshots of the particles flowing in the inlet and outlet regions of the boxcar-type electrodes, respectively (movies are shown in SI).

al. 1997; Gorre-Talini et al. 1998; Malgaretti 2013; Kowalic and Bishop et al. 2016). However, techniques that only employ the fluid dynamic force cannot be used to control and change the timing of particles passing a specific position and the time interval. Generating a traveling wave accurately in a microchannel can be challenging in terms of installing the technique in the microfluidic system.

We developed a technique that can control the timing and interval (spacing) between the particles and cells in the microchannel flow by periodically exerting forces on the particles over space and time (see Fig.

1). In our previous work, we applied a dielectrophoretic force to the particles and Jurket cells using ladder-type electrodes (Tatsumi et al. 2019). Regions of dielectrophoretic force accelerating and decelerating the particles were formed periodically in the streamwise direction. The force was activated periodically over time by turning the applied voltage on and off. We demonstrated that the combination of these two schemes could align the particles and Jurket cells with equal spacing and intervals. However, the physical explanation of the convergence characteristics of the particles to the equilibrium state was not clearly explained and evaluated.

In this paper, we will discuss the principle and demonstrate the performance of the proposed technique using boxcar-electrodes. An analysis based on the perturbation theory for the one-dimensional problem will first be discussed to discuss the convergence characteristic of the particle alignment using the proposed method. The boxcar-type electrodes used in this study have a more simplified and efficient geometry than the ladder-type electrodes. It can also apply the dielectrophoretic force and control the particles over a larger area in the channel cross-section.

Figs. 1 (c) and (d) show snapshots of the particles measured at the inlet and outlet regions of the boxcar-electrode region, which demonstrates the alignment of particles in the streamwise direction as it flows through the boxcar-electrode region (movies demonstrating the particle alignment are provided in the supplementary information). We will show the accuracy of the proposed method by showing the probability density function (PDF) of the interval, velocity, and timing of the particles. The particle motion is measured, and the relationship between the particle velocity and the phase of the applied voltage signal is obtained to confirm the characteristics of the particles converging to the equilibrium state derived from the analysis. A three-dimensional numerical simulation of the dielectrophoretic force and the equation of motion of the particles is conducted to understand the motion in detail. Finally, the timing, interval, and velocity of the particles with diameters of 8, 10, and 12μm are compared to discuss the effects of some variation in the particle diameter on the accuracy and performance of the proposed technique.

2. Principle and analysis based on perturbation theory for the technique

We apply a periodic pattern of the force in the streamwise direction, which accelerates and decelerates the particle, and activate this force in cycles. The particle that deviates from the equivalent position will receive additional force to return to the equilibrium state through the combination with the on-off cycle of the spatially periodic force and the net velocity generated by the flow, that is, the particles will align with equal space in the streamwise diction.

We consider a one-dimensional problem of the force distribution and particle motion to discuss the convergence of the particles to the equilibrium state in the simplified form. As shown in Fig. 2, the force exerted on the particle decreases linearly from positive to negative in the streamwise direction for one periodic region.

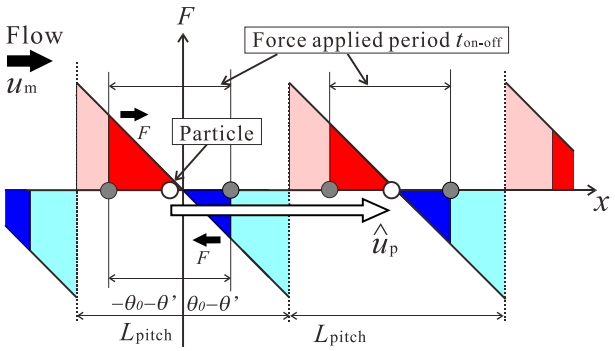

Fig. 2. Schematic of the force distribution and the force exerted on the particle when the phase deviates from the equilibrium state described in a one-dimensional model.

We first consider the condition that the flow velocity is equal to the products of the periodic length and the on-off frequency of the force, $L_{on\text{-}off}f_{on\text{-}off}$. We start from the equilibrium position at which zero work will be performed on the particle during one periodic cycle. The force is activated periodically for a certain period which corresponds to the region of $-\theta_0 \leq x \leq \theta_0$ in this case. We now assume that the phase of the particle against the equilibrium position is perturbed. In this case, the work applied to the particle during this cycle W_{DEP} can be written as Eq. (1), where ε and $\theta^{(i)}$ (i=1, 2, 3 …) are the perturbation coefficient and high-order terms for the order of i.

$$W_{DEP} = W_{DEP,0} + \frac{\partial W_{DEP}}{\partial \theta} d\theta = W_{DEP,0} + \frac{\partial W_{DEP}}{\partial \theta}\left(\varepsilon\theta^{(1)} + \varepsilon^2\theta^{(2)} + \cdots\right)$$

$$= W_{DEP,0} - 2a\theta_0\theta^{(1)}\varepsilon - 2a\theta_0\theta^{(2)}\varepsilon^2 + \cdots. \quad (1)$$

Value a is the coefficient of the relationship between x and force F in Fig. 2. $W_{DEP,0}$ is zero, and if we consider only the first-order correction term, W_{DEP} is written as Eq. (2).

$$W_{DEP} \cong -2a\theta_0\theta'. \quad (2)$$

We then consider the particle kinetic energy U. Having $\hat{u}_{p,0}$ be the particle average velocity in one periodic region at equilibrium, U can be expressed as Eq. (3) with the perturbation series.

$$U = \frac{1}{2}m\hat{u}_{p,0}^2 + \left.\frac{\partial U}{\partial \hat{u}_p}\right|_0 d\hat{u}_p + \frac{1}{2}\left.\frac{\partial^2 U}{\partial \hat{u}_p{}^2}\right|_0 d\hat{u}_p{}^2 + \cdots = \frac{1}{2}m\hat{u}_{p,0}^2 + m\hat{u}_{p,0}\left(\varepsilon\hat{u}_p^{(1)} + \varepsilon^2\hat{u}_p^{(2)} + \cdots\right) + \cdots. \quad (3)$$

m is the mass of the particle. Therefore, deviation from the equilibrium state ΔU can be written as

$$\Delta U \cong m\hat{u}_{p,0}\hat{u}_p', \quad (4)$$

where $\hat{u}_p'$ is the deviation from the velocity of the equilibrium state $\hat{u}_{p,0}$.

We then define the variation of $\hat{u}_p'$ in one periodic region as $d\hat{u}_p'$. The variation of U due to this change, defined here as dU, can be expressed as Eq. (5).

$$dU \cong m\hat{u}_{p,0}d\hat{u}_p'. \quad (5)$$

As dU should be equal to the work applied to the particle in one periodic region $dW_{DEP} \cong -2a\theta_0\theta'$, the following relationship can be derived:

$$d\hat{u}_{\mathrm{p}}{}' = -\frac{2at_{\mathrm{on-off}}}{m}\,\theta'. \tag{6}$$

Here, we assumed that θ_0 is proportional to $\hat{u}_{\mathrm{p},0}t_{\mathrm{on-off}}$, where $t_{\mathrm{on\text{-}off}}$ is the period of one cycle and is equal to $1/f_{\mathrm{on\text{-}off}}$.

We will now define the variation of θ' in one periodic region as $\Delta\theta'$. $\Delta\theta'$ can be approximated by $\Delta\theta' \cong \hat{u}_{\mathrm{p}}{}'t_{\mathrm{on-off}}$. If one periodic length is negligibly small compared with the total length of the region of interest, this can be rewritten as $\hat{u}_{\mathrm{p}}{}' = -d\theta'/dt$. Substituting this relationship in Eq. (6), the intermitted characteristics of the applied force and particle motion can finally be expressed as the differential equation shown in Eq. (7).

$$\frac{d^2\theta'}{dt^2} = -\frac{2a}{m}\theta'. \tag{7}$$

Eq. (7) gives us an oscillatory solution for θ'.

The particle also receives the drag force from the fluid on the basis of the relative velocity with the fluid. When the particle is in the equilibrium (periodic) state, the periodic force exerted on the particle in the region of $-\theta_0 \leq x \leq \theta_0$ keeps the particle in this region also working against the fluid drag force. On the other hand, in the case of the displacement θ', the fluid drag force affects the particle as a damping force in relation to the additional particle motion attributed to θ'. This effect can be added to Eq. (7) as a damping term, which gives a solution converging to θ'=0.

As mentioned previously, this formula, which holds for $-\theta_0 < x < \theta_0$, is based on the condition that the flow velocity is equal to $L_{\mathrm{pitch}}f_{\mathrm{on\text{-}off}}$. However, this discussion can also be applied for flow velocities different from $L_{\mathrm{pitch}}f_{\mathrm{on\text{-}off}}$. In this case, the equilibrium position in the periodic region will move to apply additional work on the particle and have the particle obtain the velocity of $\hat{u}_{\mathrm{p}} = L_{\mathrm{pitch}}f_{\mathrm{on-off}}$. The convergence characteristic derived previously should not be affected by this movement in the phase of the equilibrium position. Therefore, we can get the controlled particle velocity $u_{\mathrm{p}}{}^{*}=L_{\mathrm{pitch}}f_{\mathrm{on\text{-}off}}$, and the controlled time interval between the particles $1/f_{\mathrm{on\text{-}off}}$.

3. Experimental Method

Boxcar-type electrodes were patterned on the channel bottom wall, and the ground electrode covered the entire area of the channel top wall, as shown in Fig. 1. The top and bottom walls were glass substrates on which platinum electrodes were patterned. The layer between the two glass substrates was made of SU-8 (Microchem, Su-8 3050) and was fabricated using a soft lithography process. The microchannel was patterned on the Su-8 layer. The width, length, and pitch of the traverse electrode were 50 μm, 10 μm, and 50 μm, respectively. The channel height and width were 51 μm and 200 μm, respectively. The top glass substrate was attached to the Su-8 layer by thermal bonding. The two substrates were aligned and then pressed using the hot pressing machine (AS ONE: MNP-001) for 30min at the temperature of 150°C.

The fluid was supplied to the channel by a pump driven by pressurized air. Three inlets were set at the

inlet of the microchannel, where the particle suspended solution was supplied to the center inlet while the side flows were used to control the overall flow rate. The rail-type electrodes (Tatsumi et al. 2016) were placed downstream of the channel inlet, by which the particles were focused by dielectrophoretic force and guided to the inlet of the boxcar-electrode region.

Polystyrene microparticles with diameters of 8, 10, and 12 μm (Thermoscientific Co., 4208A, 4210A, 4212A) were used in the measurements. The particles were mixed in Milli-Q water at a concentration of 0.2 %. Sodium lauryl sulfate was added to the solution at a concentration of 0.1 wt% to prevent the adhesion of particles to the wall. The flow rate was 3.9 μL/min, giving an average flow velocity of 6.4 mm/s. The Reynolds number based on the channel hydraulic diameter and particle size of 12μm in this case, were 0.37 and 0.055, respectively.

We applied an alternating current (AC) voltage to the electrode using a function generator with a peak-to-peak voltage of $V_{p\text{-}p}$ = 16.8 V and frequency of f_V = 10 MHz. This voltage was turned on and off periodically with a frequency of $f_{on\text{-}off}$ = 125 Hz. The duty rate of applied voltage was fixed at 50%. AC of f_V = 10 MHz was used to reduce the formation of the electric-double layer on the surface of the electrode and avoid the voltage drop and the generation of electroosmotic flow. The AC electric field will also cause Joule heating, by which the fluid temperature can increase several degrees in the boxcar-electrode region under the present flow and electric condition. The temperature increase is small to generate an electrothermal flow affecting the particle motion (Ramos et al. 1998), and the effect on biological cells is negligible as long as the flow rate is reasonably high.

The motion of the particles was recorded using a high-speed video camera and microscope. The frame rate and resolution of the measurement were 10,000 fps and 0.88 μm, respectively. The particle position and velocity were obtained from a series of images using motion analysis software (Library Co. Ltd., Move-tr/2D ver. 7.90).

4. Numerical Method

The equation of motion of the particles was solved considering the effects of the dielectrophoretic force F_{DEP} and the hydrodynamic forces exerted on the particles. The electric field was first obtained by solving the Poisson equation for the relationship between the electric potential and charge using COMSOL Multiphysics (ver. 4.3a: COMSOL Inc.). Figure 3 (a) shows the computational domain. The height and width of the domain were 50 μm and 200 μm, which were equal to the channel height and width, respectively. The streamwise length is 100 μm, which is twofold of the periodic length L_{pitch}. AC electric potential was applied to the electrodes while electrical insulation conditions was set at other boundaries.

The electric field gradient obtained by the computation was then applied to the multipole method using a third-order Clausius–Mossotti function to calculate the F_{DEP} distribution (Washizu and Jones 1994; Jones and Washizu 1996). We employed the multipole method to calculate the F_{DEP} accurately in such area where the area size of the electric field distribution in the microchannel is close to the particle size (Tatsumi et al.

2014).

The hydrodynamic forces were based on the Stokes force for spheres, to which the models of Goldman et al. (Goldman et al. 1967a, b), and Cooley and O'neill (Cooley and O'neill 1969) considering the effects of the velocity gradient and the wall were applied. The validation of the present method is made in the authors' previous work by comparing the results of the computation and measurement for the particle motion in a periodic unit of ladder-type electrodes, which resulted in a good agreement (Tatsumi et al. 2019).

5. Results and Discussion

5.1 Motion and alignment characteristics of the particles

Figs. 1 (c) and (d) demonstrate that the particles can be focused at the centerline of the boxcar-electrodes and evenly spaced in the streamwise direction. We will show the numerical results of the dielectrophoretic (DEP) force distribution exerted on the particles if located at that position and the particle velocity distribution to examine the particle motion in the boxcar-electrode region. Figs. 3 (b) and (c) represent the distributions of the x-direction component of the DEP force $F_{\mathrm{DEP},x}$ on the x-y plane at z/H=0.1, and on the x-z plane at y/W=0, respectively. Figs. 3 (d) and (e) show the distribution of the y-component of the DEP force $F_{\mathrm{DEP},y}$ on y-z plane at x/L=0 and z-component $F_{\mathrm{DEP},z}$ on the x-z plane at y/W=0, respectively.

The spanwise DEP force $F_{\mathrm{DEP},y}$ moves the particles toward the centerline of the boxcar-electrode and focuses the particles at the centerline. The DEP force $F_{\mathrm{DEP},z}$ shown in Fig. 3 (e) gives a positive value near the traverse electrode, while it shows a negative value in the region between the traverse electrodes. Therefore, the height of the particle increases and decreases if the voltage is applied to the electrode when the particle flows over these regions. As the flow streamwise velocity increases in the direction from the channel wall to the channel center, the variation in the particle height accelerates and decelerates the particle in addition to the effect of the $F_{\mathrm{DEP},x}$. The sum of the DEP force and fluid dynamic force exerted on the particle in the equilibrium state F_{x} in relation to the streamwise position $x_{\mathrm{p}}/L_{\mathrm{pitch}}$ is shown in Fig. 3 (f). Fig. 3 (g) shows the streamwise velocity of the particle u_{p} in relation to $x_{\mathrm{p}}/L_{\mathrm{pitch}}$. The "on" and "off" description in the figure shows the period when the voltage is turned on and off. The acceleration region is generated at the traverse electrode and immediately downstream of the traverse electrode, and the deceleration region appears further downstream near the middle of the region between the traverse electrodes. It should be noted that the F_{x} becomes zero shortly after the voltage is turned off as the particle velocity becomes equal to the flow velocity due to the fluid drag force.

Fig. 4 shows the distribution of the particle velocity averaged over one periodic region $\hat{u}_p$. The value of the abscissa axis n_{b} is the order number of the periodic regions (transverse electrode) of the boxcar-electrode. Figs. 4 (a) and (b) represent the results measured in the region near the inlet and outlet of the boxcar-electrode. At the inlet, $\hat{u}_{\mathrm{p}}$ shows a deviation from the target value $u_{\mathrm{p}}^{*} = L_{\mathrm{pitch}} f_{\mathrm{on-off}}$ (which is

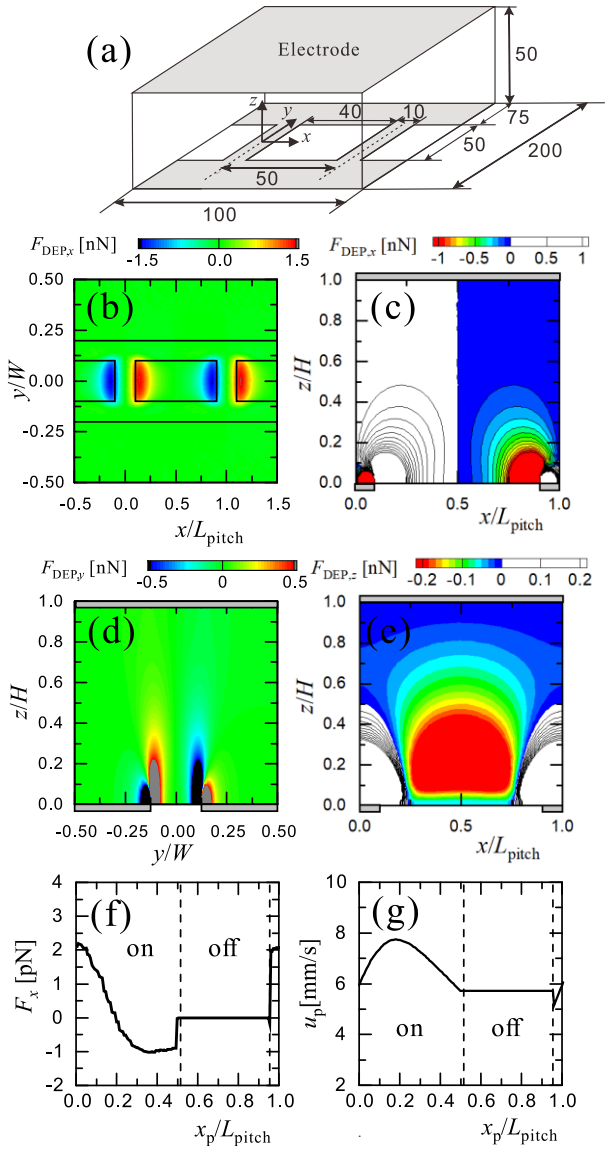

Fig. 3. (a) Computation domain. (b) and (c) Distributions of the x-direction component of the DEP force $F_{DEP,x}$ on the x-y plane at z/H=0.1, and on the x-z plane at y/W=0. (d) y-component DEP force $F_{DEP,y}$ on y-z plane at x/L_{pitch}=0. (e) z-component DEP force $F_{DEP,z}$ on the x-y plane at y/W=0. (f) Sum of the DEP force and fluid dynamic force exerted on the particle in relation to the streamwise position x_p/L_{pitch}. (g) Particle streamwise velocity in relation to x_p/L_{pitch}.

6.25 mm/s for the present condition) shown by the line in the figure. As the particle flows downstream, $\hat{u}_p$ fluctuates and then approaches the value u_p^*. By the time the particle reaches n_b~50, $\hat{u}_p$ converges, and has a constant value, as shown in Fig. 4 (b).

As shown in Fig. 3 (f), the force exerted on the particle shows a distribution similar to that considered in Section 2. Particles whose position deviates from the equilibrium receive an additional force, which converges them to the equilibrium. In the measurement, we should be able to observe a correlation between

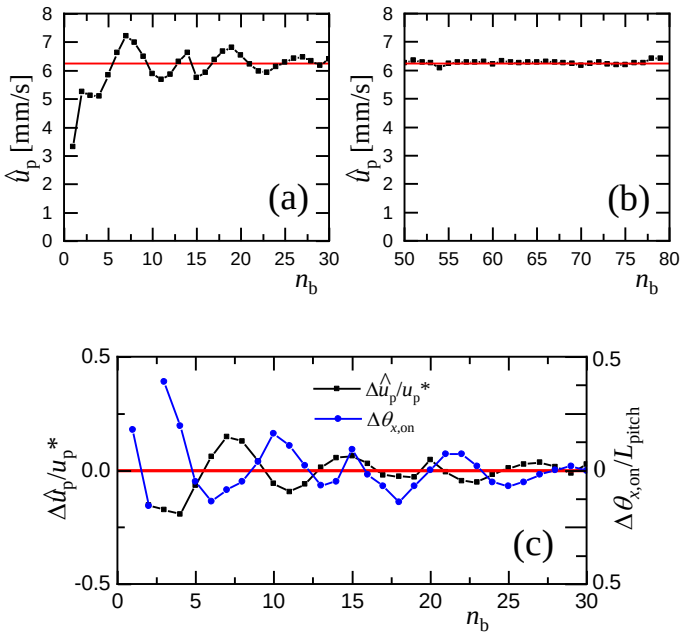

Fig. 4. Distribution of particle velocity averaged in one periodic region $\hat{u}_p$ in relation to the streamwise direction measured at the (a) inlet and (b) outlet regions of the boxcar-electrode, and (c) comparison between the particle velocity $\hat{u}_p$ and spatial phase $\theta_{x,on}$ deviations from the equivalent position.

the displacements of the particle position and velocity from their equilibrium states during the convergence process. Therefore, we synchronized the timing of the camera exposure with the on-off cycle of the voltage applied to the electrode and measured the relationship between the particle velocity and the phase difference.

Fig. 4 (c) shows the distributions of the $\Delta\hat{u}_p/u_p^*$ and $\Delta\theta_{x,on}/L_{pitch}$ against n_b. The value $\Delta\hat{u}_p$ is the particle velocity difference from the equilibrium state $\Delta\hat{u}_p = \hat{u}_p - u_p^*$. The value $\Delta\theta_{x,on}$ is the phase difference from the equilibrium state, that is, the distance between the positions of the particle of interest and the particle at equilibrium state, both at the moment when the voltage rises. The particle position for the equilibrium state was obtained from the measurement conducted near the outlet of the boxcar-electrode at which the particle showed periodic motion. The value of $\Delta\hat{u}_p$ increases in the region for $\Delta\theta_{x,on}<0$, and decreases for $\Delta\theta_{x,on}>0$. Therefore, a negative correlation between the gradient of $\Delta\hat{u}_p$ and $\Delta\theta_{x,on}$ is obtained in the distribution making both $\Delta\hat{u}_p$ and $\Delta\theta_{x,on}$ converge to zero, which agrees well with the discussion on the model made in Section 2.

5.2 Performance evaluation

We measured the probability density function (PDF) of the values for the particle to evaluate the performance of the proposed technique. Figs. 5 (a) to (d) show the probability density function of Δt and $\Delta\hat{u}_p$ for particles measured at the first and last boxes of the boxcar-electrodes, respectively. Δt is the time

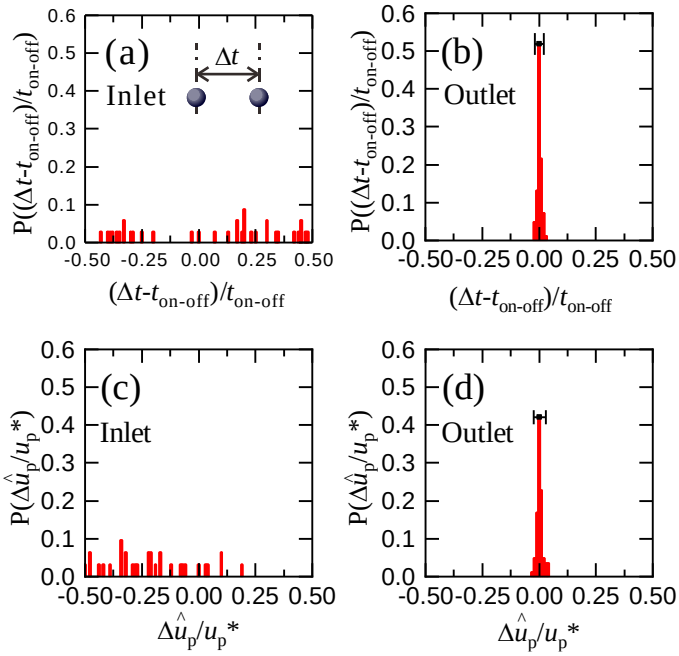

Fig. 5. Probability density function for the time interval between particles Δt and deviation of the particle velocity from target value $\Delta\hat{u}_p$: (a) and (b) PDFs of $(\Delta t\text{-}t_{on\text{-}off})/t_{on\text{-}off}$ at the inlet and outlet of the boxcar-electrode region, and (c) and (d) PDFs of $\Delta\hat{u}_p/u_p^*$ at the inlet and outlet.

interval between the two particles, and the graphs show the deviation of Δt from the period of the voltage on-off cycle $t_{on\text{-}off} = 1/f_{on\text{-}off}$. In Figs. 5 (a) and (c), both values $(\Delta t - t_{on\text{-}off})/t_{on\text{-}off}$ and $\Delta\hat{u}_p/u_p^*$ at the inlet show scattered distributions. However, $(\Delta t - t_{on\text{-}off})/t_{on\text{-}off}$ and $\Delta\hat{u}_p/u_p^*$ show a sharp maximum peak at the value of zero at the outlet, respectively. The error bar in the graph represents the 95% confidence interval of each distribution. The confidence intervals of $(\Delta t - t_{on\text{-}off})/t_{on\text{-}off}$ and $\Delta\hat{u}_p/u_p^*$ fall inside the range of ±1.9% and ±2.6%, respectively.

We will now evaluate the performance of the proposed technique in controlling the timing of the particles. Figs. 6 (a) to (d) show snapshots of the particles in the outlet region for different time phases $\theta_{t,on}$. $\theta_{t,on}$ is the temporal phase difference from the time of the voltage rise. The relative positions of the particles to the traverse electrodes are the same for the particles in each figure. As the particle motion is synchronized with the on-off cycle of the voltage, the position of the particle in the periodic region can be predicted from the applied voltage signal. In other words, this indicates that we can control the timing when the particle passes a certain position in the channel by changing the phase of the applied voltage.

We measured the time difference between the signal rise of the voltage and the time when the particles crossed the middle of the boxcar-electrode region (x/L_{pitch}=0.5) to evaluate the performance of timing control using the proposed technique. The PDFs of $\theta_{t,on}(x/L_{pitch}=0.5)/t_{on\text{-}off}$ is shown in Figs. 6 (e) and (f). At the inlet of the boxcar-electrode, the PDF shows a scattered distribution, indicating that the timing in

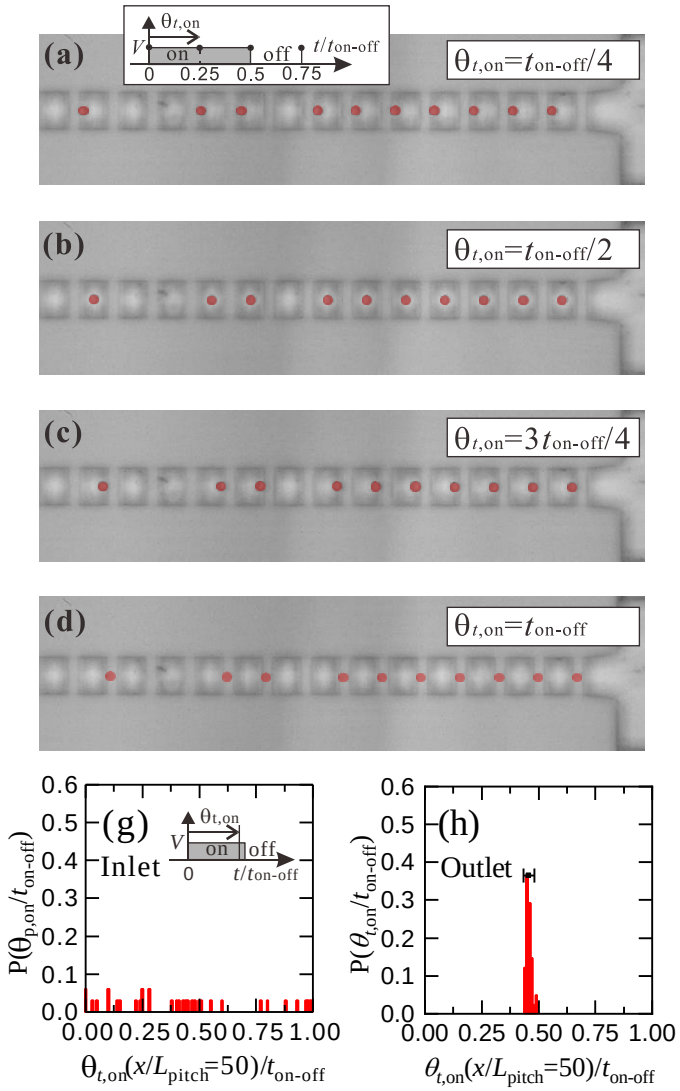

Fig. 6. (a) – (d) Aligned particles in the outlet region of the boxcar-electrode in different phases. $\theta_{p,on}$ is the time (phase) difference from the rising edge of the applied voltage. (e) and (f) PDFs for $\theta_{t,on}/t_{on\text{-}off}$ of x/L_{pitch}=50 at the inlet and outlet of the boxcar-electrode region.

relation to the applied voltage is random. On the other hand, at the outlet, the PDF shows a maximum peak at $\theta_{t,on}(x/L_{pitch}=0.5)/t_{on\text{-}off}$ =0.46, with a 95% confidence interval within the range of ±2.5%.

5.3 Phase-shift characteristics

As discussed in Section 2, the particle velocity $\hat{u}_p$ converges to the target value u_p^* even when the flow velocity differs from the target value. In this case, the additional force will exert on the particles to accelerate and decelerate the particles by having an additional phase shift with the particles over time and space. We measured the spatial phase of the particles at the time of the voltage drop, defined as $\theta_{x,off}$ for mean flow velocity u_m=5.4 mm/s, 6.4 mm/s, and 7.7 mm/s. The results are shown in Fig. 7 together with

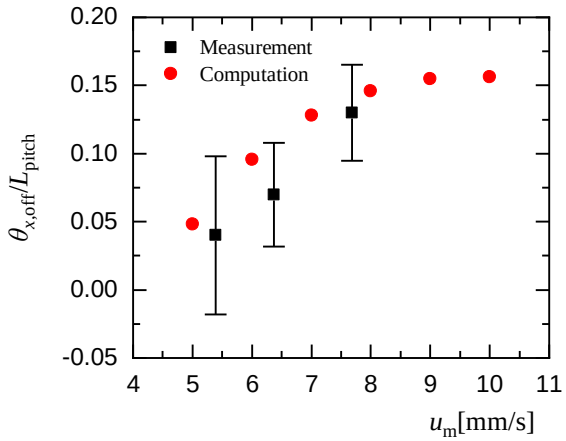

Fig. 7. Effect of the average flow velocity on the position of the particle at the voltage fall $\theta_{x,off}$ with the origin located at the middle of the boxcar-electrode.

the numerical computation for u_m = 5.0–10.0 mm/s for comparison.

The value of $\theta_{x,off}$ increases as the u_m increases, showing that the time phase delays, or the spatial phase shifts downstream as the flow velocity increases. As shown in Fig. 3 (f), first a positive force and then negative force exerts on the particle during the period of the voltage application. When the phase delays, the time of the negative force applied to the particle increases. This balance with the increase in the fluid drag force attributed to the increase in the average flow velocity.

The average values and 95% confidence interval of the particle velocity $\hat{u}_p$ for u_m= 5.4, 6.4, and 7.7 mm/s were 6.37mm/s ±7.3%, 6.27 mm/s ±2.6%, and 6.28 mm/s ±6.1%, respectively, which shows that we can maintain the average particle velocity at the target value $L_{pitch}f_{on\text{-}off}$ with some variation in the flow velocity. It is worth mentioning here that the flow velocity and $L_{pitch}f_{on\text{-}off}$ can be increased to larger value as long as the flow is in laminar regime and the two values meet the condition mentioned previously. The periodic force can affect the particle relative position to converge to the equilibrium (periodic) state even in higher flow rate. However, the time when the DEP force is applied to the particle during one period decreases as the flow rate increase, and the number of periodic units required for the particle to flow over and converge to the equilibrium state will increase in this case.

5.4 Effect of particle size variation

We carried out further measurements using particles with diameters of 8 and 10 μm to evaluate the effect of the particle size variation on the alignment, velocity, and timing control characteristics. Furthermore, we conducted a measurement for the mixed aqueous solution of 8, 10, and 12 μm diameter particles. The probability density functions of the time interval between the particles $(\Delta t - t_{on\text{-}off})/t_{on\text{-}off}$, particle velocity $\Delta\hat{u}_p/u_p^*$, and the phase difference from the voltage rise $\theta_{t,on}(x/L_{pitch}=0.5)/t_{on\text{-}off}$ are shown in Fig. 8. The average value, the range of the 95% confidence interval σ, and the number of samples n are

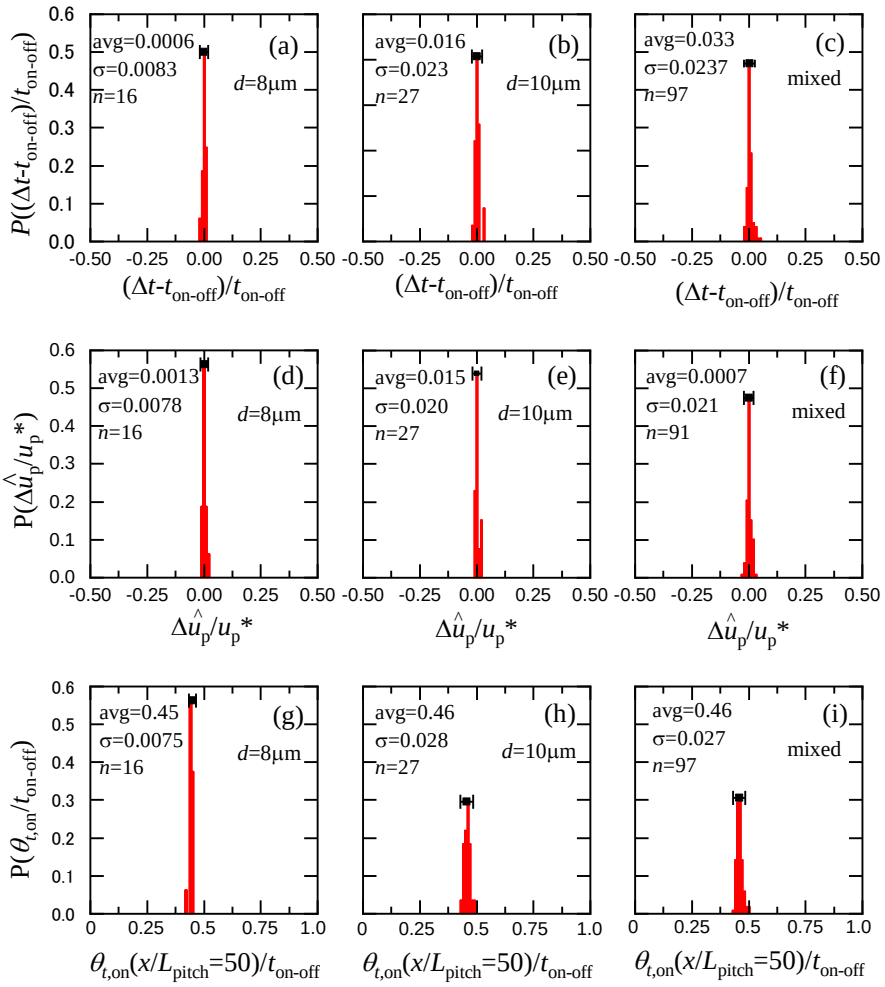

Fig. 8. Probability density function of the time interval between particles Δt, particle velocity $\Delta\hat{u}_p$, and phase based on the voltage rise $\theta_{t,on}$ for the case of particle size of d=8, 10μm, and the mixed solution of particles with diameters of 8, 10, and 12μm.

shown in the figure. The PDFs for the values of $\Delta t/t_{on\text{-}off}$ and u_p/u_p* concentrate at zero for all particles with negligibly small deviations that fall within the range of less than ±2.1%. The PDFs of $\theta_{t,on}(x/L_{pitch}=0.5)/t_{on\text{-}off}$ for all particles, focus at the same value with a deviation of less than ±3.1%, reflecting the high accuracy of the timing control.

Although the examined range was several micrometers in this study, the results of having particles with different diameters converging to the same position and timing are notable but reasonable. The particle size affects the magnitude of the dielectrophoretic force and fluid drag force. Smaller particles will receive smaller forces, which may decrease the function to make the particle converge to the equilibrium position. Therefore, a longer duration and length may be necessary to align the particles. However, if the force distribution shows a similar pattern between particles of different sizes, the equilibrium position at which the positive and negative work balances and the total work is equal to zero during one periodic cycle would

be the same. In this case, the particles focus at the same position and time.

6. Conclusions

We proposed a novel technique that can align the particles with equal space and interval as they flow in the microchannel by exerting forces on the particles in periodic form over space and time using the dielectrophoretic force generated by the boxcar-electrodes. The one-dimensional model based on the perturbation analysis and the measurement results proved that the particles would converge to the equilibrium state, and the interval between two particles and the particle velocity would be equal to $L_{\text{pitch}}f_{\text{on-off}}$ and $t_{\text{on-off}}$, respectively. The measurement showed that we could control the particle interval, particle velocity, and the timing of particles crossing a specific position within an accuracy of ±2.6%, 1.9%, and 2.5%, respectively. The control accuracy of these values could be maintained when the particle diameter varied in the range of approximately ±20% or when the flow velocity changed within a certain range. Although we used the dielectrophoretic force to generate the periodic force, the principle of the technique proposed here can be applied to different forces to control the particles, cells, droplets, and other objects in the flow.

Funding

This work was supported by the Japan Society for the Promotion of Science KAKENHI Grant Number 17K18841 and partially by Micro/Nano Fabrication Hub at Kyoto University of "Low-Carbon Research Network" funded by the Ministry of Education, Culture, Sports, Science and Technology (MEXT), Japan.

Conflicts of interest

The authors declare that they have no conflict of interest.

Availability of data and material

The datasets generated during and/or analyzed during the current study are available from the corresponding author on reasonable request.

Supplementary Information

Video S1: The movie of 12 μm particles entering the boxcar-type electrode region with random intervals.

Video S2: The movie of 12 μm particles aligned and flowing with even spaces near the outlet of the boxcar-type electrode region.

References

Abate AR, Chen CH, Agresti JJ, Weitz DA (2009) Beating Poisson encapsulation statistics using close-packed ordering Lab on a Chip **9**: 2628-2631.

Afshar R, Moser Y, Lehnert T, Gijs MAM (2011) Three-dimensional magnetic focusing of superparamagnetic beads for on-chip agglutination assays. Analytical Chemistry **83**: 1022-1030.

Ahn B, Lee K, Lee H, Panchapakesan R, Xu L, Xu J, Oh KW (2011) Guiding, distribution, and storage of trains of shape-dependent droplets. Lab on a Chip. **11**: 3915-3922.

Baret JC, Miller OJ, Taly V, Ryckelynck M, El-Harrak A, Frenz L, Rick C, Samuels ML, Hutchison BH, Agresti JJ, Link DR, Weitz DA, Griffiths AD (2009) Fluorescence-activated droplet sorting (FADS): efficient microfluidic cell sorting based on enzymatic activity. Lab on a Chip **9**: 1850-1858.

Borromeo M, Marchesoni F (1998) Brownian surfers. Physics Letters A **249**: 199-203.

Chen T, Wu TH, Kung YC, Teitell MA, Chiou PY (2013) 3D pulsed laser-triggered high-speed microfluidic fluorescence-activated cell sorter. Analyst **24**: 7308-7315**.**

Chen R, Wang C, He Z (2019) Abnormal transport behaviors in traveling wave system. Chaos, Solitons and Fractals **126**: 116-121.

Cheung KC, Di Berardino M, Schade-Kampmann G, Hebeisen M, Pierzchalski A, Bocsi J, Mittag A, Ta´rnok A (2010) Microfluidic impedance-based flow cytometry. Cytometry Part-A **77A**: 648-666.

Chung AJ, Gossett DR, Di Carlo D (2013) Three dimensional, sheathless, and high-throughput microparticle inertial focusing through geometry-induced secondary flows. Small **9**: 685-690.

Čižmár T, Šiler M, Zemánek P (2006) An optical nanotrap array movable over a milimetre range. Applied Physics B **84**: 197-203.

Coakley WT, Bardsley DW, Grundy MA (1989) Cell manipulation in ultrasonic standing wave fields. Journal of Chemical Technology & Biotechnology **44**: 43-62.

Constantin A (2006) The trajectories of particles in Stokes waves. Inventions Mathematics **166**: 523-535.

Cooley MDA, O'neill ME (1969) On the slow motion generated in a viscous fluid by the approach of a sphere to a plane wall or stationary sphere. Mathematica **16**: 37-49.

Cui L, Holmes D, Morgan H (2001) The dielectrophoretic levitation and separation of latex beads in microchips. Electrophoresis **22**: 3893-3901.

D'Avino G, Maffettone PL (2020) Numerical simulations on the dynamics of trains of particles in a viscoelastic fluid flowing in a microchannel. Meccanica **55**: 317-330.

Di Carlo D, Irimia D, Tompkins RG, Toner M (2007) Continuous inertial focusing, ordering, and separation of particles in microchannels. PNAS **104**: 18892-18897.

Dietsche C, Mutlu BR, Edd JF, Koumoutsakos J, Toner M (2019) Dynamic particle ordering in oscillatory inertial microfluidics. Microfluidics and Nanofluidics **23**: 83.

Edd JF, Di Carlo D, Humphry KJ, K¨oster S, Irimia D, Weitzb DA, Toner M (2008) Controlled encapsulation of single-cells into monodisperse picolitre drops. Lab on a Chip **8**: 1262-1264.

Faucheux LP, Bourdieu LS, Kaplan PD, Libchaber AJ (1995) Optical thermal ratchet. Physical Review Letters **74**: 1504-1507.

Fedele F, Chandre C, Farazmand M (2016) Kinematics of fluid particles on the sea surface. Hamiltonian theory. Journal of Fluid Mechanics **801**: 260-288.

Feynman RP (1949) The theory of positrons. Physical Review **76**: 749-759.

Fiedler S, Shirley SG, Schnelle T, Fuhr G (1998) Dielectrophoretic sorting of particles and cells in a microsystem. Analytical Chemistry **70**: 1909-1915.

Gao Y, Magaud P, Baldas L, Lafforgue C, Abbas M, Colin S (2017) Self‐ordered particle trains in inertial microchannel flows. Microfluidics and Nanofluidics **21**: 154.

Garcés-Chévez V, Dholakia K, Spalding GC (2005) Extended-area optically induced organization of microparticles on a surface. Applied Physics Letters **86**: 031106.

Garcia M, Pennathur S (2019) A model for inertial particles in curvilinear flows. Microfluidics and Nanofluidics **23**: 63.

Giudice FD, D'Avino G, Greco F, Maffettone PF, Shen AQ (2018) Fluid viscoelasticity drives self-assembly of particle trains in a straight microfluidic channel. Physical Review Applied **10**: 064058.

Goldman AJ, Cox RG, Brenner H (1967) Slow viscous motion of a sphere parallel to a plane wall I: Motion through a quiescent fluid. Chemical Engineering Science **22**: 637-651.

Goldman AJ, Cox RG, Brenner H (1967) Slow viscous motion of a sphere parallel to a plane wall II: Couette flow. Chemical Engineering Science **22**: 653-660.

Gorre-Talini L, Spatz JP, Silberzan P (1998) Dielectrophoretic ratchets. Chaos **8**: 650-656.

Guo F, Ji XH, Liu K, He RX, Zhao LB, Guo ZX, Liu W, Guo SS, Zhao XZ (2010) Droplet electric separator microfluidic device for cell sorting. Applied Physics Letters **96**: 193701.

Hu X, Lin J, Ku X (2019) Inertial migration of circular particles in Poiseuille flow of a power-law fluid. Physics of Fluids **31**: 073306.

Hu X, Lin J, Chen D, Ku X (2020) Stability condition of self‐organizing staggered particle trains in channel flow. Microfluidics and Nanofluidics **24**: 25.

Hughes MP (2002) Strategies for Dielectrophoretic Separation in laboratory-on-a-chip systems. Electrophoresis **23**: 2569-2582.

Jones TB, Washizu M (1996) Multipolar dielectrophoretic and electrorotation theory. Journal of Electrostatics **7**: 121-134.

Jűlicher F, Ajdari A, Prost J (1997) Modeling molecular motors. Reviews of Modern Physics **69**: 1269-1281.

Kemna EWM, Schoeman RM, Wolbers F, Vermes I, Weitz DA, Van den Berg A (2012) High-yield cell ordering and deterministic cell-in-droplet encapsulation using Dean flow in a curved microchannel. Lab on a Chip **12**: 2881-2887.

Koss BA, Grier DG (2003) Optical peristalsis. Applied Physics Letters **82**: 3985-3987.

Kowalik M, Bishop JM (2016) Ratcheted electrophoresis of Brownian particles. Applied Physics Letters **108**: 203103.

Lagus TP, Edd JF (2013) High-throughput co-encapsulation of self-ordered cell trains: cell pair interactions in microdroplets. RSC Advances **3**: 20512-20522.

Laurell T, Petersson F, Nilsson A (2007) Chip integrated strategies for acoustic separation and manipulation of cells and particles. Chemical Society Reviews **36**, 492-506.

Lewis OL, Guy RD (2017) Analysis of peristaltic waves and their role in migrating Physarum plasmodia. Journal of Physics D: Applied Physics **50**: 284001.

Lozano C, Bechinger C (2019) Diffusing wave paradox of phototactic particles in traveling light pulses. Nature Communications **10**: 2495.

Lu X, Liu C, Hu G, Xuan X (2017) Particle manipulations in non-Newtonian microfluidics: A review. Journal of Colloid and Interface Science **500**: 182-201.

Magnasco MO (1993) Forced thermal ratchets. Physical Review Letters **71**: 1477-1481.

Malgaretti P, Pagonabarraga I, Rubi JM (2013) Confined Brownian ratchets. The Journal of Chemical Physics **138**: 19490.

Morgan H, Green NG, Hughes MP, Monaghan W, Tan TC (1997) Large-area travelling-wave dielectrophoresis particle separator. Journal of Micromechanics and Microengineering **7**: 65-70.

Oakey J, Applegate RW, Arellano E, Di Carlo D, Graves SW, Toner M (2010) Particle focusing in staged inertial microfluidic devices for flow cytometry. Analytical Chemistry **82**: 3862-3867.

Ramos A, Morgan H, Green N G, Castellanos A (1998) Ac electrokinetics: a review of forces in microelectrode structures. J. Physics D: Applied Physics **31**: 2338-2353.

Rousselet J, Salome L, Ajdari A, Prost J (1994) Directional motion of Brownian particles induced by a periodic asymmetric potential. Nature **370**: 446-447.

Sun T, Green NG, Gawad S, Morgan H (2007) Analytical electric field and sensitivity analysis for two microfluidic impedance cytometer designs. IET Nanobiotechnol **1**: 69-79.

Sun YY, Yuan XC, Ong LS, Bu J, Zhu SW, Liu R (2007) Large-scale optical traps on a chip for optical sorting. Applied Physics Letters **90**: 031107.

Schoeman RM, Kemna EWM, Wolbers F, Van den Berg A (2014) High-throughput deterministic single-cell encapsulation and droplet pairing, fusion, and shrinkage in a single microfluidic device. Electrophoresis **35**: 385-392.

Shields CW, Reyes CD, López GP (2015) Microfluidic cell sorting: a review of the advances in the separation of cells from debulking to rare cell isolation. Lab on a Chip **15**: 1230-1249.

Tatsumi K, Kawano K, Okui H, Shintani H, Nakabe K (2016) Analysis and measurement of dielectrophoretic manipulation of particles and lymphocytes using rail-type electrodes. Medical Engineering and Physics. **38**: 24-32.

Tatsumi K, Kawano K, Shintani H, Nakabe K (2019) Particle timing control and alignment in

microchannel flow by applying periodic force control using dielectrophoretic force. Analytical Chemistry **91**: 6462-6470.

Tierno P, Straube AV (2016) Transport and selective chaining of bidisperse particles in a travelling wave potential," European Physical Journal E **39**: 54.

Washizu M, Jones TB (1994) Multipolar dielectrophoretic force calculation. Journal of Electrostatics **33**: 187-198.

Wood CD, Evans SD, Cunningham JE, O'Rorke R, Wälti C, Davies AG (2008) Alignment of particles in microfluidic systems using standing surface acoustic waves. Applied Physics Letters **92**: 044104.

Xuan X, Zhu J, Church C (2010) Particle focusing in microfluidic devices. Microfluidics and Nanofluidics **9**:1-16.

Yan S, Zhang J, Yuan D, Li W (2017) Hybrid microfluidics combined with active and passive approaches for continuous cell separation. Electrophoresis **38**: 238-249.

Yigit S, Wang H, Han S-I, Cho Y., Han A (2020) Acoustofluidic microdevice for precise control of pressure nodal positions. Microfluidics and Nanofluidics **24**: 52.

Yuan D, Sluyter R, Zhao Q, Tang S, Yan S, Yun G, Li M, Zhang J, Li W (2019) Dean-flow-coupled elasto-inertial particle and cell focusing in symmetric serpentine microchannels. Microfluidics and Nanofluidics **23**:41.

Zemánek P, Jonáš A, Jákl P, Ježek J, Šerý M, Liška M (2003) Theoretical comparison of optical traps created by standing wave and single beam. Optics Communications **220**: 401-412.

Zhang S, Wang Y, Onck P, Toonder J (2020) A concise review of microfluidic particle manipulation methods. Microfluidics and Nanofluidics **24**: 24.

Zhang X, Zheng D, Zhong W (2019) One-dimensional mass transport with dynamic external potentials. Chinese Physics B **28**: 020505.

Zhu J, Tzeng TRJ, Hu G, Xuan X (2009) DC dielectrophoretic focusing of particles in a serpentine microchannel. Microfluidics and Nanofluidics **7**: 751-756.